SUPPORTING INFORMATION

Structural Dimensionality Governing CO_2/C_2H_2 Separation in MWW Zeolites

Ang Li[1], Xiao-Xia Zhang[1], Yuqi Zhang[2], Mariya Shamzhy[2], Xing-Zhe Guo[1], Wan Yan[1], Bingwen Li[3,*], Xuzhi Hu[1,*] and Rongsheng Cai[1,*], Feng Zhou[1]

[1]*State Key Laboratory of Solid Lubrication, Lanzhou Institute of Chemical Physics, Chinese Academy of Sciences, Lanzhou, 730000, PR China*

[2]*Department of Physical and Macromolecular Chemistry, Charles University, Hlavova 8, 128 43 Prague 2, Czech Republic*

[3]*Shandong Key Laboratory of Biophysics, Institute of Biophysics, College of Chemistry and Chemical Engineering, Dezhou University, Dezhou 253023, PR China*

Experimental Section

Chemicals and materials:

Sodium aluminate ($NaAlO_2$, 55% Al_2O_3, 45% Na_2O), silica nanoparticles, (10-20 nm), tetrabutylammonium hydroxide solution (TBAOH, 40%), tetraethyl orthosilicate (TEOS), sodium hydroxide solution (50%), hexamethyleneimine (HMI) were purchased from Aladdin Reagent Co., Ltd. Deionized water was used for the described experiments. All chemicals were used without further treatment.

Synthesis of MCM-56:

The synthesis gel for MCM-56 were prepared with following chemical composition: 1 SiO_2: 0.04 Al_2O_3: 0.093 Na_2O: 0.3 HMI: 16 H_2O.[1, 2] Typically, 0.9 g 50% NaOH solution and 4 g HMI were added into 39 g H_2O and then mixed. 1.05 g sodium aluminate was added into the mixing solution. After the solid was dissolved fully, 9.3 g silica nanoparticles (10-20 nm) were added in batches. The final white reaction gel was vigorously stirred at room temperature for 2 hours to make it fully homogenous and then transferred into Teflon-lined autoclaves and heated under rotation at 145 °C for 38 hours. The obtained solid was collected and washed with distilled water and EtOH 3 times until the filtrate was neutral (pH~ 7). Then the zeolites were dried at 65 °C overnight. For sorption experiment, the prepared MCM-56 was grinded and calcined at 550 °C for 6 hours with a temperature ramp of 1 °C /min for further use.

Synthesis of MCM-22p and MCM-22:

The molar ratio of synthesis gel for MCM-22p was as follow: 30 SiO_2: 1 Al_2O_3: 2.5 Na_2O: 10 HMI: 580 H_2O.[3] In a typical synthesis, 1.868 g 50% NaOH solution and 9.92 g HMI were added into 61.256 g H_2O. 1.943 g sodium aluminate was added into the solution under mixing. After the

solid was dissolved fully, 60 g colloidal silica (Ludox-LS30, 30% in water) was added dropwise while vigorously mixing. After stirring for 2 hours at room temperature, the gel was transferred into Teflon-lined autoclaves and heated under rotation at 143 °C for 96 hours. The as-synthesized sample was then filtered and washed with distilled water and EtOH until neutralized. The collected solid was finally dried at 65 °C overnight. To prepare MCM-22, the MCM-22p needs to be calcined at 550 °C for 6 hours with temperature ramp of 1 °C /min.

Synthesis of MCM-36:

MCM-36 was prepared as the procedure in previous report, based on the post-modification of swollen MCM-22p.[4] The MCM-22p synthesized above was dried and then swelling with 20 g of the 25 wt% ion-exchanged OH form of CTAB solution over night at room temperature. CTAB was dissolved in water to prepare 25 wt% solutions and then ion-exchanged to the OH^- form using Ambersep 900 OH resin. Typically, 70 g of resin was used for ion-exchange of 100 g of the original solution of surfactant for swelling. The product was isolated by centrifugation and washed with distilled water 2 times. The final solid was dried at 65 ^oC overnight. The MCM-36 was prepared via a pillaring process of the swollen sample. In a typical synthesis, 0.5 g of dried swollen MCM-22p solids from above were mixed with 15 g TEOS and heated under reflux at 85-95 ^oC overnight. Then, the products were collected by centrifugation. After decantation of the supernatant TEOS, the tube was kept upside down for 6–24 h to drain and evaporate residual TEOS in case of amorphous silica phase in the final product. The as-obtained solids were then washed with water and dried at 65 ^oC. Final calcination was done at 550 ^oC for 6 h with a ramping rate of 1 ^oC/min.

Exfoliation of MCM monolayer:

The colloidal MWW monolayer suspension was obtained by a mild chemical exfoliation of as-synthesized MCM-56 at room temperature.[5] In a typical preparation, 1 g uncalcined MCM-56p

was dispersed into 10 g 10% TBAOH solution and stirred vigorously for 1.5 hours at room temperature. Afterwards, the mixture was transferred and centrifuged at 10000 rpm for 40 minutes. Then the supernatant (upper liquid) was dropped and wasted, and using the apropriate amount of water (typically for 1 g MCM-56, 30 g distilled water is used) to redisperse the precipitate (down solid). The obtained residue mixture was stirred overnight at room temperature and centrifuged again. The supernatant was piped out carefully and collected as the colloidal MWW monolayer suspension. The residue solid can be re-exfoliated to increase the yield. To purify the colloidal MWW monolayer suspension, dialysis can be done with Dialysis membranes from regenerated cellulose (Dialysis membranes "visking", obtained from BKMan Co., Ltd., MWCO 14000 Da, pore size 1.5-2.0 nm.) In a typical dialysis, the colloidal MWW monolayer suspension was loaded into proper size dialysis membrane bags and well-sealed, then the dialysis bag was transferred into certain amount of water. (1 g colloidal zeolite solutions in 30 g distilled water). The dialysis was performed overnight at room temperature, and the final pH values of both colloidal solution and outside water are recorded. The final concentration of the colloidal MWW monolayer suspension was confirmed after drying and calcination of a certain amount of colloidal solution at 550 ^{o}C. In this case, the concentration of dialyzed colloidal MWW monolayer suspension was 18.5 mg zeolite/ 1 g solution. For sorption use, the MWW monolayers were freeze-dried and then calcined at 550 ^{o}C for 6 hours, with a ramping rate of 1 ^{o}C/min.

Physisorption

All gas adsorption isotherms were measured on a Quantachrome Autosorb-iQ by the static volume method. All samples were degassed and actived using Micromeritics SmartVac Prep at 300 °C under a vacuum for 8 h before the sorption measurements. The surface area S_{BET} was evaluated using the Brunauer−Emmett−Teller (BET) method and the adsorption data in the range of a relative pressure from $p/p_0 = 0.05 - 0.25$. The t-plot method was applied to determine the volume

of micropores (V_{mic}), external and mesoporous surface area ($S_{ext+mes}$) of the sample via Harkins–Jura model with a t value of 0.8-1.3. The adsorbed amount at a relative pressure p/p_0 = 0.950 reflects the total adsorption capacity and pore volume (V_{tot}).

Fitting of unary isotherm data

The isosteric heat of adsorption (Q_{st}) was calculated based on Clausius–Clapeyron relation for quantifying the adsorption enthalpy (ΔH_{ads}) due to its direct link to experimentally measurable parameters. Q_{st} was calculated under the constraint of constant adsorbed amount (n) at isosteric condition using the dependence of equilibrium pressure (p) on temperature (T):

$$Q_{st} = RT^2\left(\frac{\partial lnp}{\partial T}\right)_n \tag{S1}$$

Thermodynamically, Q_{st} is rigorously defined as the negative of the differential molar enthalpy of adsorption ΔH_{ads}, offset by a term RT:

$$Q_{st} = -\Delta H_{ads} + RT \tag{S2}$$

The unary isotherms for C_2H_2 and CO_2 adsorbed in zeolites were measured at two different temperatures 273 K, and 298 K. The isotherms were fitted with excellent accuracy using the single-site Langmuir-Fruendlich model, where we distinguish two distinct adsorption sites A:

$$q = \frac{q_{sat,A} b_A p^{\nu_A}}{1 + b_A p^{\nu_A}} \tag{S3}$$

In eq (S3), the Langmuir-Freundlich parameters b_A are both temperature dependent

$$b_A = b_{A0}\exp\left(\frac{E_A}{RT}\right) \tag{S4}$$

In eq 错误!未找到引用源。, E_A are the energy parameters associated with sites A, respectively.

The unary isotherm fit parameters are provided in 错误!未找到引用源。.

Table S1. Single-site Langmuir-Fruendlich fits for guest molecules in mww-monolayer.

	Site A		
	$\frac{q_{A.sat}}{\text{mol kg}^{-1}}$	$\frac{E_A}{\text{kJ mol}^{-1}}$	ν_A
C_2H_2	6.49	52.40	0.33
CO_2	7.06	38.14	0.49

Table S2. Single-site Langmuir- Fruendlich fits for guest molecules in MCM-22.

	Site A		
	$\frac{q_{A.sat}}{\text{mol kg}^{-1}}$	$\frac{E_A}{\text{kJ mol}^{-1}}$	ν_A
C_2H_2	4.17	36.86	0.54
CO_2	4.07	33.14	0.74

Table S3. Single-site Langmuir-Fruendlich fits for guest molecules in MCM-56.

	Site A		
	$\frac{q_{A.sat}}{\text{mol kg}^{-1}}$	$\frac{E_A}{\text{kJ mol}^{-1}}$	ν_A
C_2H_2	3.38	36.37	0.31
CO_2	3.60	33.91	0.40

Table S4. Single-site Langmuir-Fruendlich fits for guest molecules in MCM-36.

	Site A		
	$\frac{q_{A.sat}}{\text{mol kg}^{-1}}$	$\frac{E_A}{\text{kJ mol}^{-1}}$	v_A
C_2H_2	4.14	32.75	0.61
CO_2	3.22	29.96	0.79

Selectivity Prediction for Binary Mixture Adsorption

Ideal adsorbed solution theory (IAST) was used to predict binary mixture adsorption from the experimental pure-gas isotherms. The experimental isotherm data for pure C_2H_2, and CO_2 were fitted using a single-site Langmuir equation model:

$$\boldsymbol{q} = \mathrm{a}\,\frac{b * p^c}{1 + b * p^c}$$

Where q and p are adsorbed amounts and the pressure of component i, respectively.

The adsorption selectivities for binary mixtures of C_2H_2/CO_2, defined by

$$S_{\mathrm{i/j}} = \frac{x_{\mathrm{i}} * y_{\mathrm{j}}}{x_{\mathrm{j}} * y_{\mathrm{i}}}$$

were respectively calculated using the Ideal Adsorption Solution Theory (IAST). Where x_i is the mole fraction of component i in the adsorbed phase and y_i is the mole fraction of component i in the bulk.

***In-situ* FT-IR investigation**

To investigate the interaction of CO2 and C2H2 with MCM-22 and MWW-monolayer zeolites, in situ FTIR spectroscopic study was performed at 298 K. Self-supporting zeolite wafers (8 - 12 mg·cm-2) were prepared and activated in situ at 723 K under vacuum (6 × 10-6 Torr) for 4 h to remove physisorbed water. After cooling to 298 K, dose-by-dose adsorption of CO2 or C2H2 was carried out by introducing successive doses of the gas (0.004 mmol g-1 of zeolite). Following each dose, the sample was equilibrated for 10 min prior to spectral acquisition. Spectra were collected on a Nicolet iS50 spectrometer equipped with a DTGS detector by averaging 64 scans at a resolution of 4 cm-1. All spectra were normalized to a constant sample density (10 mg·cm-2). Gas-phase spectra were recorded separately and subtracted as background.

For competitive adsorption experiments, a 50/50 (v/v) CO2/C2H2 mixture was introduced into the in situ cell at a total pressure of 12 Torr. Gas-phase spectra were again used as background. Zeolite spectra were recorded every 1 min immediately after exposure to the mixture for a total duration of 2 h.

The changes in the surface chemistry occurring upon the exfoliation of MCM-22 layers, including the nature and strength of acid sites and their distribution among internal and external surface, were studied using FTIR-monitored thermodesorption of probe molecules with different kinetic diameters: pyridine (Py, 0.57 nm) and 2,6-di-tert-butylpyridine (DTBPy, 0.79 nm). The FTIR experiments were performed following the recently revisited transmission-mode protocol for quantitative analysis of acidity in zeolites.[6] Infrared spectra were collected at room temperature (128 scans and resolution of 4 cm^{-1}) using a Nicolet™ iS50 FTIR spectrometer equipped with DTGS detector and processed with OMNIC software. Samples were prepared as self-supporting wafers using a Trystom H-62 hydraulic press at up to 40 MPa, with a mass-to-surface ratio of 8-12 g/cm^2. Prior to analysis, samples were activated under vacuum (5×10^{-6} Torr) using the same

conditions as before the adsorption tests to ensure that the acid sites detected under these conditions are directly comparable to the performance characteristics. Py and DTBPy, were adsorbed from the vapor phase at 423 K for 20 min, under 3.5 Torr (Py) or equilibrium vapor pressure (DTBPy). Following adsorption, samples were treated under vacuum to remove physisorbed probe molecules at 423 K for 20 min (Py) or 60 min (DTBPy). Acid site concentrations were calculated using molar absorption coefficients and protocols from previous report for Py and for DTBPy.[5, 7, 8] Thermodesorption of Py was carried out at 723 K for 20 min and the fraction of strong BAS and LAS was estimated as the ratio of the characteristic bands at 723 K and 423 K as reported.[9]

Theoretical simulation

DFT calculations were carried out using the CP2K code. A mixed Gaussian and planewave basis sets were employed to the calculations. Core electrons were represented with norm-conserving Goedecker-Teter-Hutter pseudopotentials, and the valence electron wavefunction was expanded in a double-zeta basis set with polarization functions along with an auxiliary plane wave basis set with an energy cutoff of 400 Ry. The generalized gradient approximation exchange-correlation functional of Perdew, Burke, and Enzerhof (PBE) was used. Each configuration was optimized with the Broyden-Fletcher-Goldfarb-Shanno (BGFS) algorithm with SCF convergence criteria of 3×10^{-6} au. To compensate the long-range van der Waals dispersion interaction between the adsorbate and the zeolite, the DFT-D3 scheme with an empirical damped potential term was added into the energies obtained from exchange-correlation functional in all calculations.

The adsorption energy ($^{\Delta E_{ads}}$) of gas molecules in zeolite structures was defined as:

$$\Delta E_{ads} = E_{total} - (E_{zeolite} + E_{gas}) \quad (1)$$

where E_{total}, $E_{zeolite}$ and E_{gas} represented the total energy of periodic model, the energy of zeolite structure, and the energy of gas molecules, respectively. The more negative the ΔE_{ads} value, the more stable the adsorption of gas molecules within the zeolite structure.

Characterization methods

Powder X-ray diffraction (PXRD) measurements were taken using a Bruker AXS D8 Advance diffractometer with a graphite monochromator and a scintillation detector in the Bragg–Brentano geometry using CuKα radiation (with an average wavelength λ= 1.54184 Å). In a typicial stepwise scanning procedure, a step increment of 0.02° was with a dwell time of 2 seconds.

Scanning electron microscope (SEM) was measured by a Thermo-Fisher Scientific Helix 5 CS instrument without prior metal coating. For the measurement, the sample powder was separated on conductive adhesives and cut from the central part of the aggregate to form thin lamella.

Scanning transmission electron microscopy (STEM) images were acquired using a Thermo-Fisher Scientific Spectra 300 microscope equipped with a Schottky-type field emission gun at an accelerating voltage of 300 kV. Samples were finely grinded, onto carbon-coated copper grids. The sample grids were mounted on the holder and in treated with plasma (using SuPro Instrument IC150 Plasma Cleaner) prior to the measurements.

Atomic force microscopy (AFM) measurements were performed on an HR-AFM instrument (Grapes Tech., Hangzhou) under ambient conditions in tapping mode using Tap190AI-G probes (Budgetsensors). The samples were prepared by diluting in deionized water, followed by ultrasonication for 30 min, drop-casting onto freshly cleaved mica substrates, and vacuum drying for 18 h prior to imaging. The AFM images were analyzed using Gwyddion software. Before quantitative analysis, all AFM data were processed by plane-leveling (flattening) to eliminate scanner-induced tilt and background curvature, ensuring accuracy of the subsequent analysis.

All breakthrough tests were performed on the 3P mixSorb S equipments and conducted using a quartz column (0.42 cm inner diameter × 5.0 cm) manually packed with zeolite powders. The samples in the column were first activated with Helium flow (10 mL min^{-1}) for 12 h at 473 K. The mixed gas was then introduced at 298 K. After each breakthrough experiment, the sample was regenerated with Helium flow of 10 mL min^{-1} under 353 K for 4 h.

XPS data were collected on a Thermo ESCALAB 250 operated at 15 kW (monochromatic AlKa radiation,1486.6 eV).

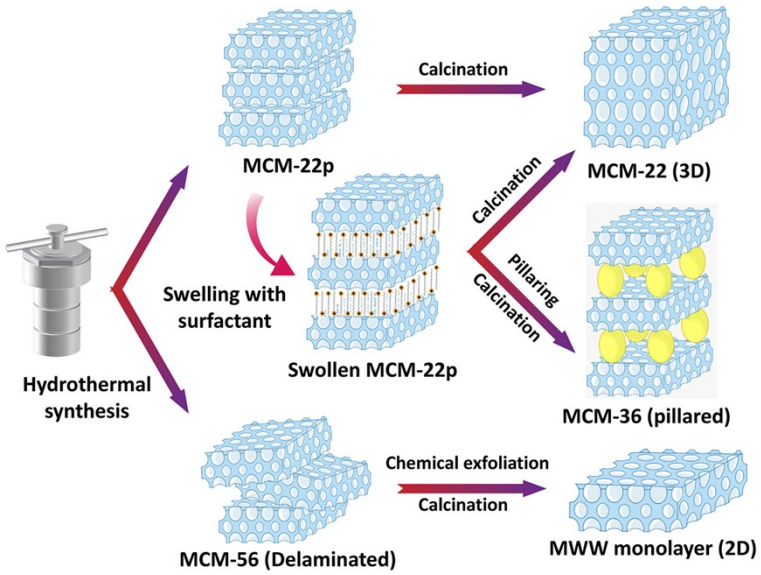

Figure S1. Schematic illustration of MWW family zeolites.

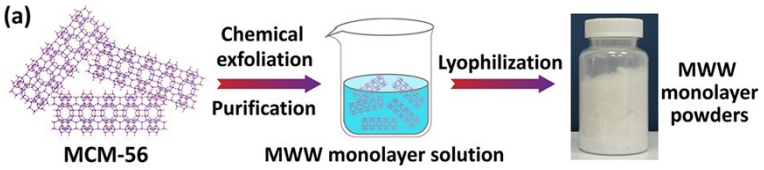

Figure S2. Schematic illustration of preparation process of for MWW monolayer powders via chemical exfoliation of MCM-56.

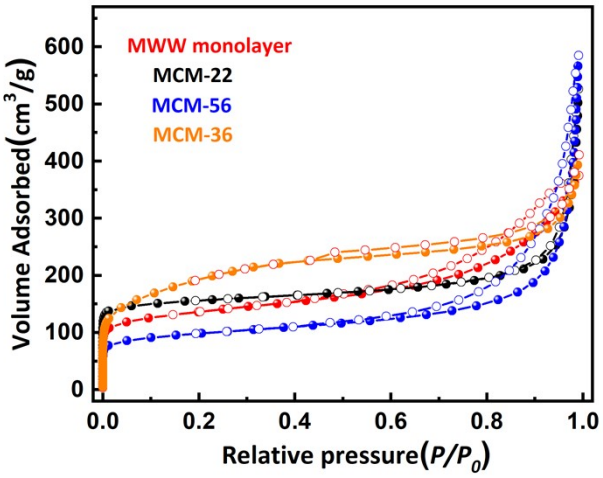

Figure S3. N_2 adsorption-desorption isotherms of MWW monolayers, MCM-22, MCM-56 and MCM-36.

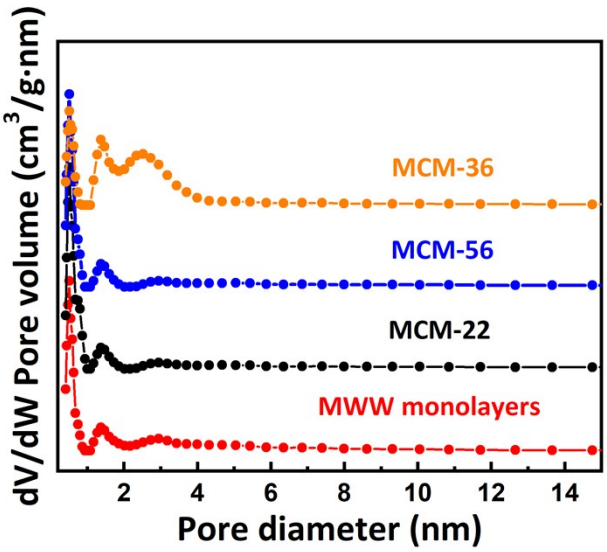

Figure S4. Pore size distribution of MWW monolayers, MCM-22, MCM-56 and MCM-36 based on N_2 adsorption-desorption isotherms.

Explanatory Note 1:

To assess the porosity of the MWW zeolites, we first measured their static volumetric pure gas isotherms, providing crucial insights into the adsorption capacity of each adsorbent. Based on the N_2 adsorption isotherms obtained at 77 K (**Fig. 1b**), the adsorption amounts (at a relative pressure of 0.99) were 374, 526, 584, and 411 cm^3/g for MWW monolayer, MCM-22, MCM-56, and MCM-36, respectively. Full isotherms including desorption branches are presented in Fig. S1. Notably, MWW monolayer and MCM-36 exhibit a combination of Type I and Type IV isotherms, indicating a combination of mesoporous and microporous structures, while MCM-22 and MCM-56 display Type I isotherms, indicative of primarily microporous characteristics according to the IUPAC definition.[10, 11] Additionally, their Brunauer-Emmett-Teller (BET) surface areas(S_{BET})and total pore volumes (V_{tot}) varied from 318 to 669 m^2/g and 0.58 to 0.88 cm^3/g, respectively (Table 1). The features and similarities in pore systems of MWW zeolites could be attributed to both their shared MWW topology and different zeolite layers connection. For MCM-22, direct connection and bonding of MWW zeolite layers create new microporosity, including bidirectional ~0.5 nm channels and 1.8×0.7 nm supercages. As for MCM-36, post-modification introduces inorganic amorphous silica as "pillars" between MWW layers. The appearance of mesoporosity was further confirmed by pore size distributions analyzed by the density functional theory (DFT) method as illustrated in **Fig. S4**. As for MWW monolayer and MCM-56, deviations in textural parameters are attributed to full (MCM-56) or partial (MWW monolayer) disorganization of zeolite layers.

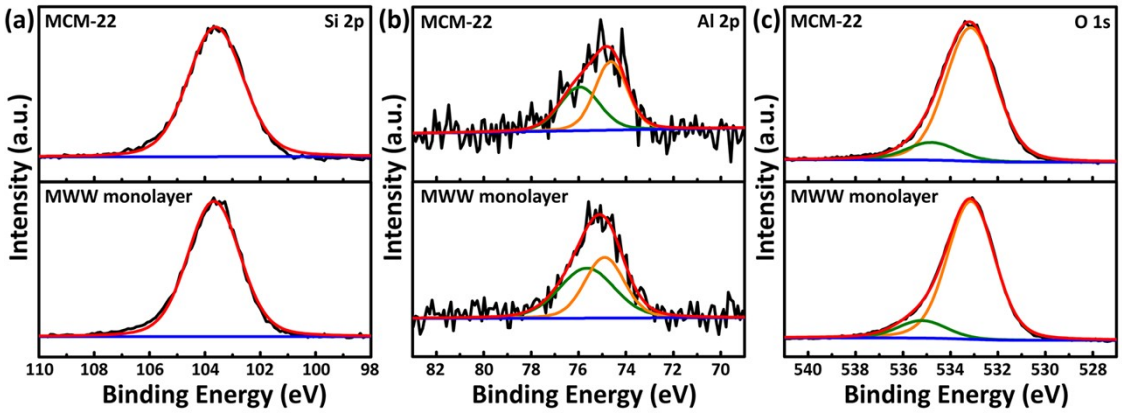

Figure S5. XPS Si 2p (a), Al 2p (b) and O 1s (c) spectra of MCM-22 and MWW monolayer after calcination.

Explanatory Note 2:

X-ray photoelectron spectroscopy (XPS) investigation on MCM-22 and MWW monolayer were conducted to unravel their surface chemical structures.[12]

The results of XPS were presented in **Fig. S5**. In general, the XPS spectra were calibrated according to C 1s peak of adventitious carbon (binding energy of 248.8 eV) on the surfaces of materials.[13, 14] The binding energy of silica species was centered at 103.6 eV but the peaks were not perfectly symmetric, which could be attributed to different crystal defects (Si-OH in this case) from the alkaline exfoliation and hydrothermal synthesis process.[15] The binding energy signal for Al 2p could be deconvolved to 2 parts of 74.6 eV and 75.7-76 eV belonged to tetrahedral framework Al site and extra-framework Al (penta-coordinated and octahedral Al), respectively.[15, 16] The difference of binding energy and Al specie ratios for MWW monolayer and MCM-22 was a result of dealumination during strong alkaline exfoliation of monolayer precursor, MCM-56. For O 1s, the peaks can be both separate as one at 533.1 eV and one at 534.9-535.3 eV.[17] The peak at 533.1 eV was allocated to the O atoms in tetrahedra units in zeolite frameworks and the broad peak at 534.9-535.3 eV were usually recognized as defects and adsorbed water species. [15]

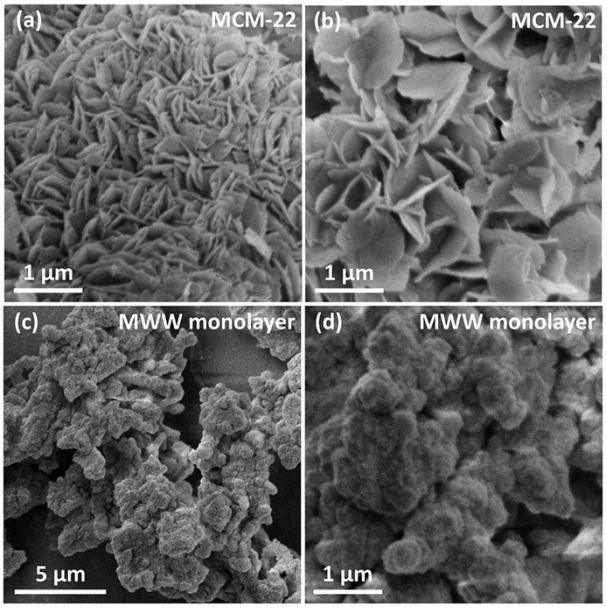

Figure S6. SEM images of MCM-22 and MWW monolayer.

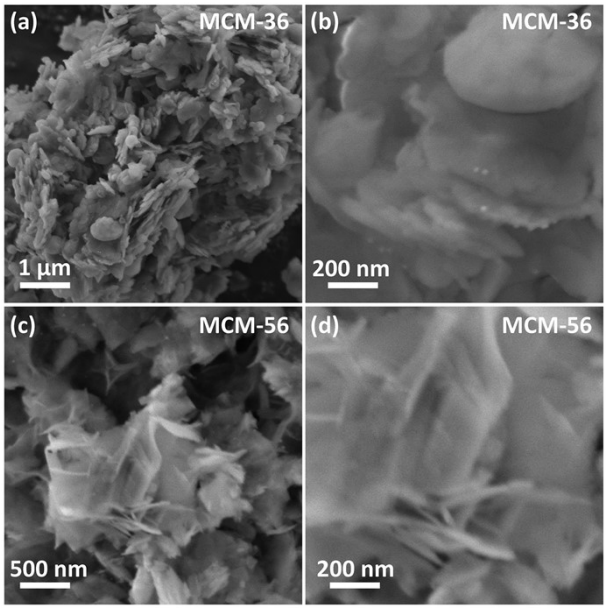

Figure S7. SEM images of MCM-36 and MCM-56.

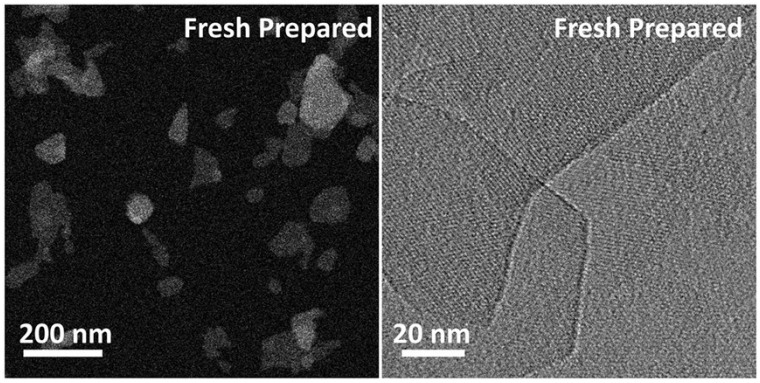

Figure S8. HAADF-STEM (left) and high-resolution TEM (right)images of fresh prepared MWW monolayer without lyophilization and calcination.

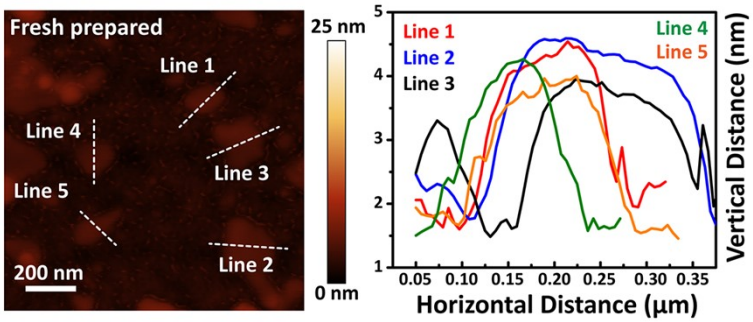

Figure S9. AFM image and horizontal-vertical distance profile of fresh prepared MWW monolayer without lyophilization and calcination.

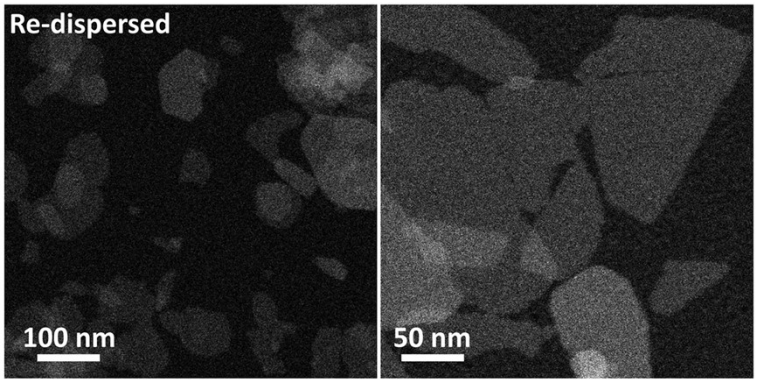

Figure S10. HAADF-STEM images of re-dispersed MWW monolayer after lyophilization and calcination.

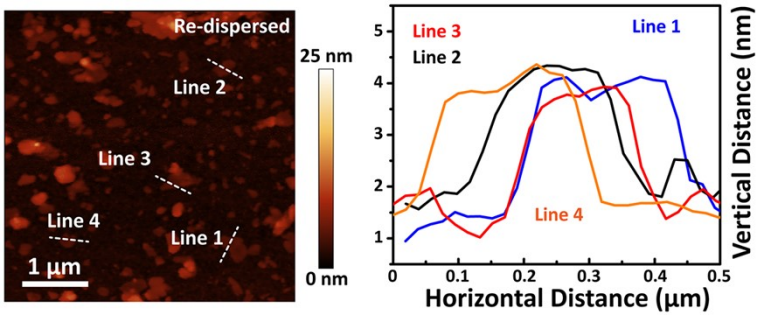

Figure S11. AFM image and horizontal-vertical distance profile of re-dispersed MWW monolayer after lyophilization and calcination.

Explanatory Note 3:

The MWW monolayer powders after lyophilization and calcination (as presented in the **Fig. S1**) can be partially re-dispersed in 1% TBAOH solution, with a weight/volume ratio of 1/200. In a typical treatment, 0.1 g MWW monolayer solid powder were dispersed in 20 mL 1% TBAOH solution. After stirring at room temperature overnight, partial MWW monolayer can be re-dispersed. In **Fig. S10&S11**, the MWW monolayer was firstly calcined at 750 °C for 6 hours and then re-dispersed in 1% TBAOH solution.

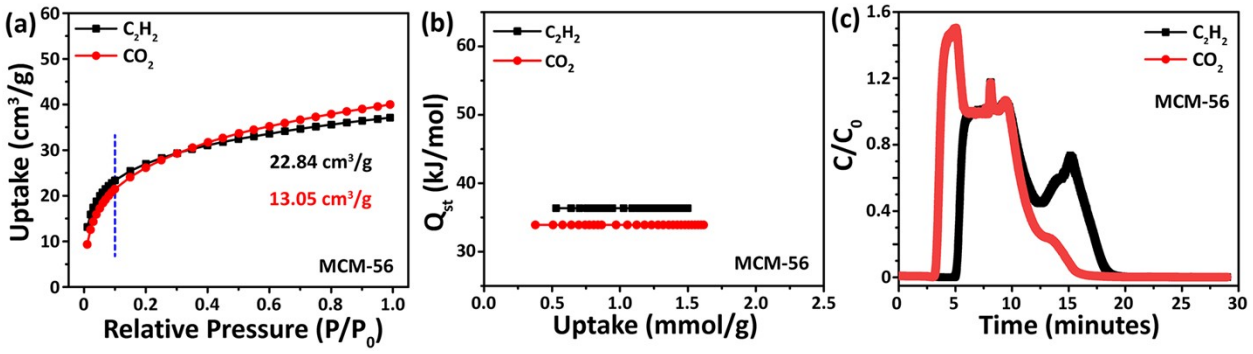

Figure S12. (a) C_2H_2 and CO_2 adsorption isotherms measured at 298 K for MCM-56, (b) Q_{st} values calculated based on Clausius-Clapeyron equation; (c) experimental dynamic competitive breakthrough curves of MCM-56 at 298 K with C_2H_2/CO_2 mixtures of 50/50 and flowrate of 2 ml/min.

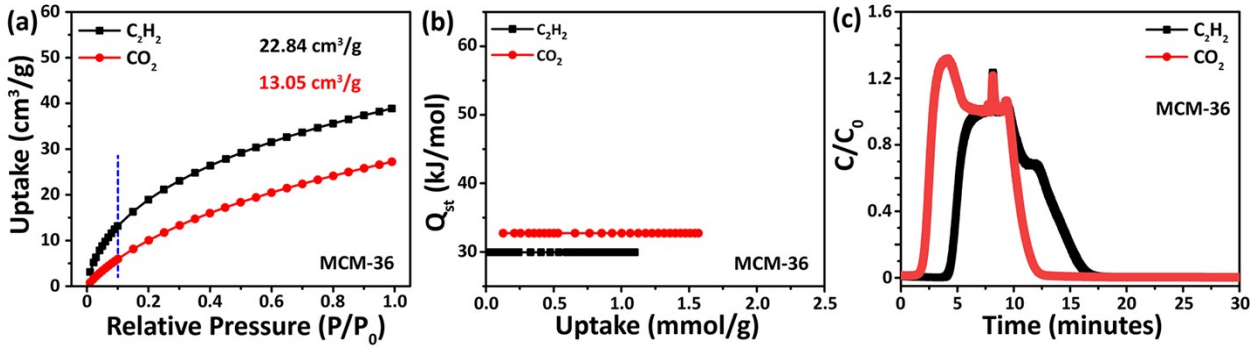

Figure S13. (a) C_2H_2 and CO_2 adsorption isotherms measured at 298 K for MCM-36, (b) Q_{st} values calculated based on Clausius-Clapeyron equation; (c) experimental dynamic competitive breakthrough curves of MCM-36 at 298 K with C_2H_2/CO_2 mixtures of 50/50 and flowrate of 2 ml/min.

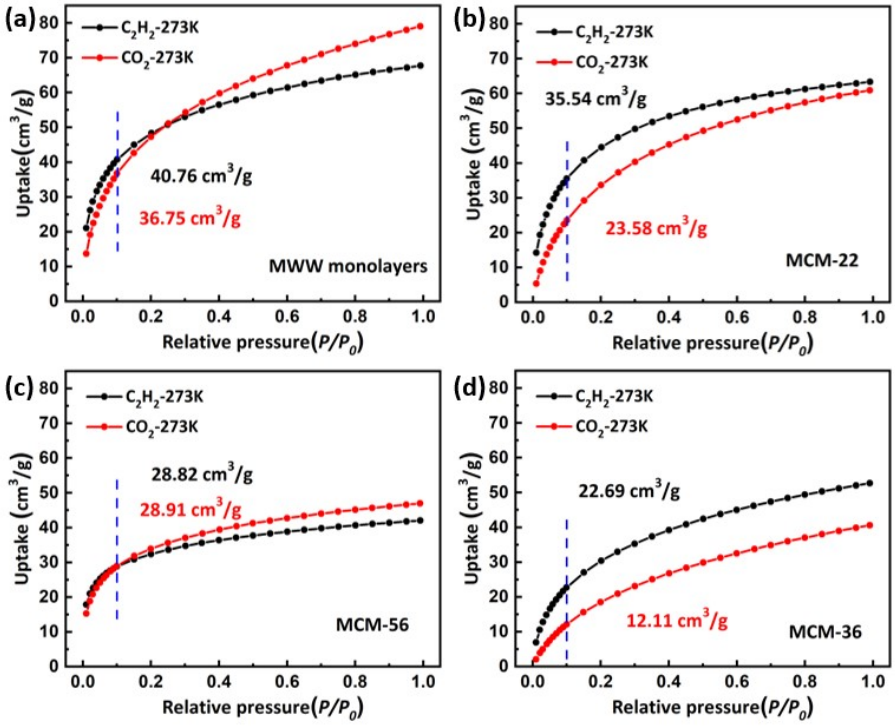

Figure S14. Adsorption isotherms of MWW monolayers (a), MCM-22 (b), MCM-56(c) and MCM-36 (d) obtained at 273 K.

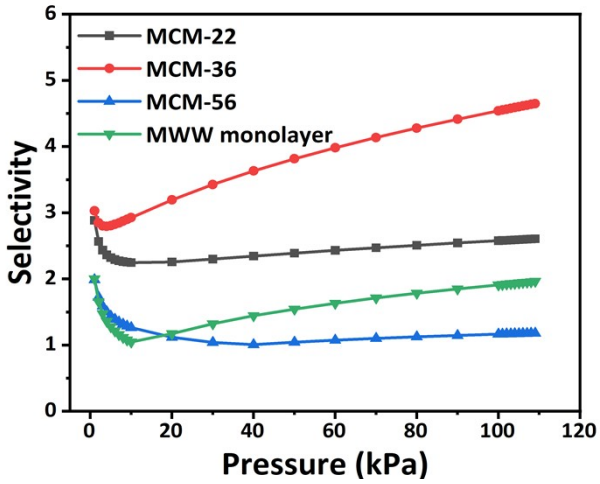

Figure S15. IAST calculations of MWW monolayers, MCM-22, MCM-56 and MCM-36 at 298 K for mixtures of C_2H_2/CO_2 (50/50).

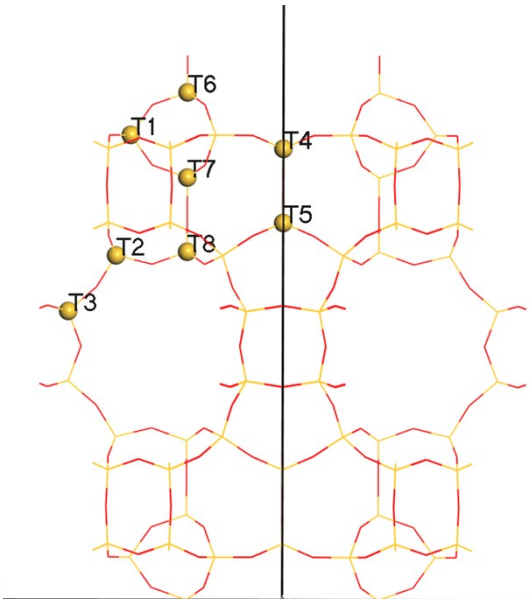

Figure S16. The T sites of **MWW** zeolite topology model along (001) direction.

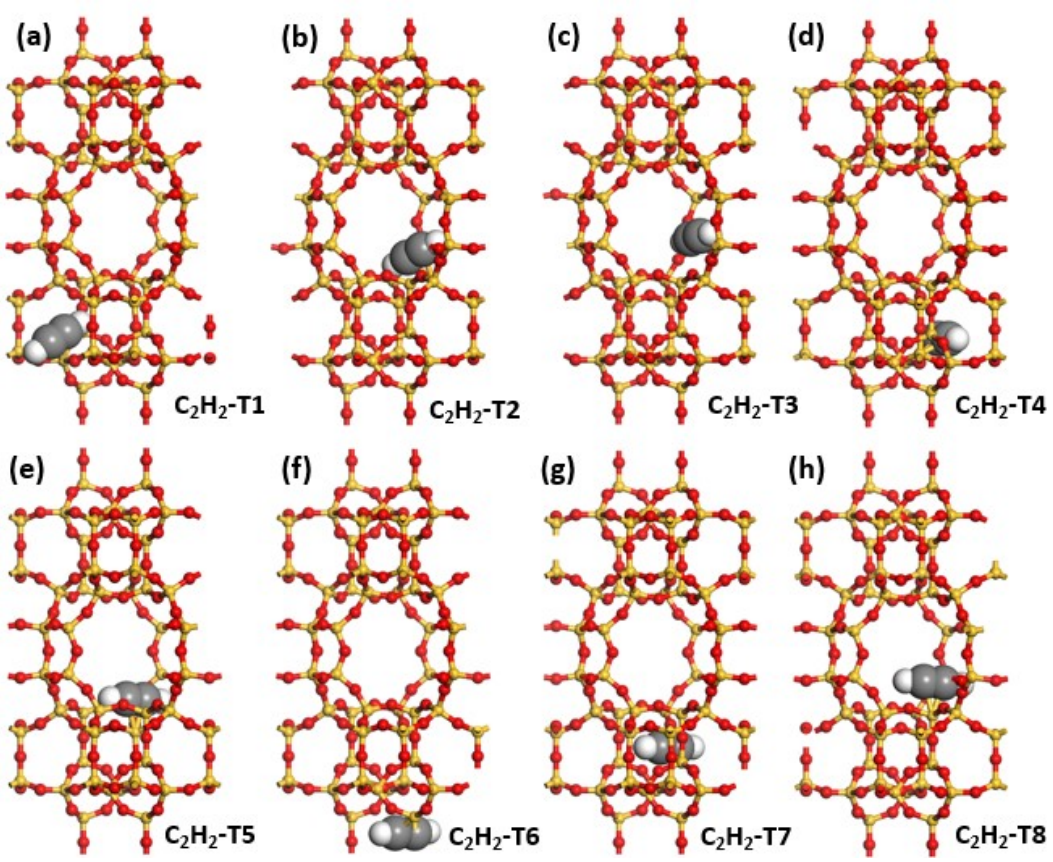

Figure S17. The simulation model of C_2H_2 molecules at different T sites in MWW model.

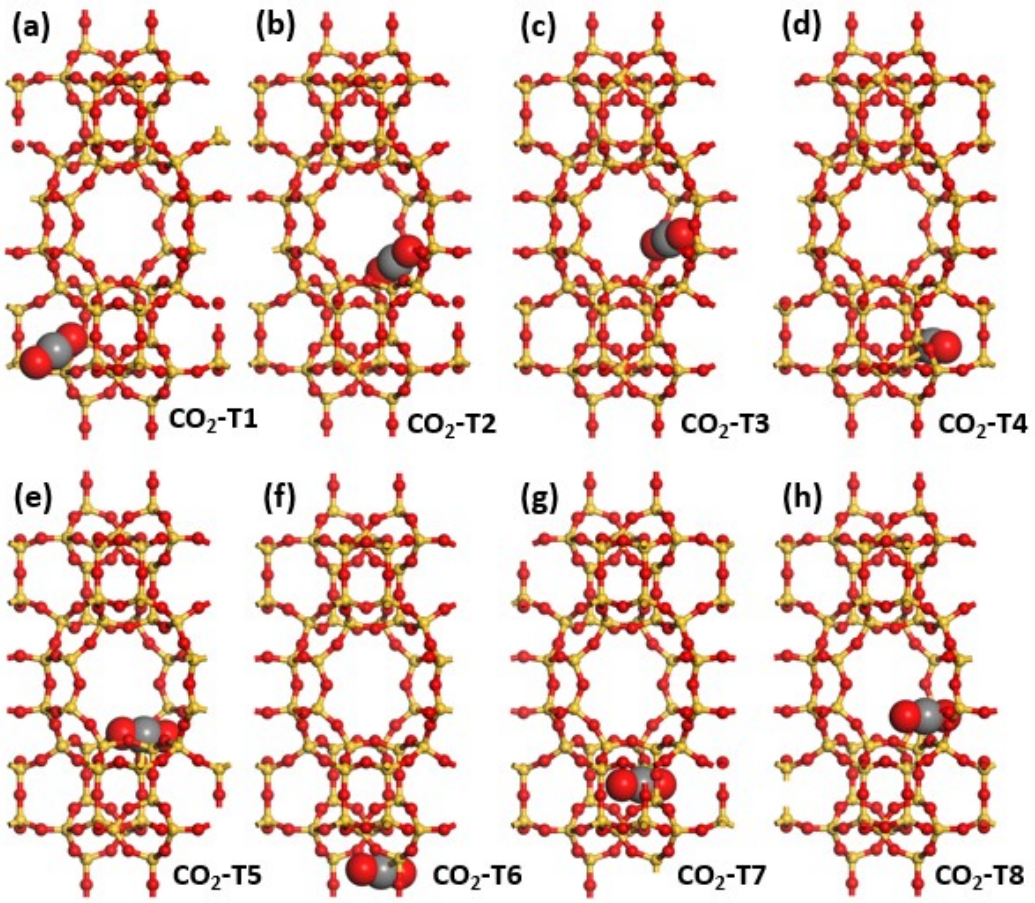

Figure S18. The simulation model of CO_2 molecules at different T sites in MWW model.

Table S5. Comparison of gas uptake and C_2H_2/CO_2 separation performance among reported CO_2-selective adsorbents.

Material	Gas uptake (mmol/g)		IAST Selectivity (CO_2/C_2H_2)	Ref
	CO_2	C_2H_2	50/50	
Cu(Qc)2	1.99	0.79	5.6	10.1002/anie.202400823
Y-bptc	2.45	1.17	4.1	10.1016/j.seppur.2022.122318
GIS (2.6)	3.51	0.04	8.5×10^{10}	10.1016/j.seppur.2024.126764
GIS (3.1)	3.5	0.59	2844	
Sr/K-HEU	2.21	0.14	38 [b]	10.1002/anie.202419091
$NaAlO_2$@MOR(0.5)	2.69	1.67	543.3 [a]	10.1002/adma.202501870
Na-CHA	4.07	3.92	1.79	10.1002/ange.202522386
K-CHA	3.51	0.62	4350	
Cs-CHA	1.44	0.15	8.10	
NaY-5.8	3.39	3.31	1.79	10.1021/jacs.5c14895
NH_4Y-5.8	3.17	3.64	3.41	
TMeA-Y-5.8	1.10	2.35	16.1	
STU-130	3.26	4.31	4.23	10.1021/acs.inorgchem.5c04160
Fe-MOF	2.49	6.33	3.59	10.1021/acs.inorgchem.2c03236
$CuZn_3(PDDA)_3(OH)$	1.94	4.20	3.3	10.1021/acsmaterialslett.2c00518
UPC-117	0.96	1.39	1.38	10.1021/acs.inorgchem.5c02031
NNM-5	0.95	2.97	16.6	10.1021/acs.chemmater.4c03017
MIL-160(Al)	4.12	9.16	6.68	10.1021/acs.chemmater.1c04168
MCM-22	1.79	2.06	2.58	**This Work**
MCM-36	1.10	1.57	4.54	
MCM-56	1.61	1.50	1.18	
MWW monolayers	2.30	2.07	1.91	

Note：[a] Kinetic selectivity. [b] Dynamic selectivity

.

References

[1] W. J. Roth, P. Chlubná, M. Kubů, D. Vitvarová, *Catal Today,* **2013**, 204, 8.

[2] G. G. Juttu, R. F. Lobo, *Microporous mesoporous mater.*, **2000**, 40, 9.

[3] A. Corma, C. Corell, J. Perezpariente, *Zeolites*, **1995**, 15, 2.

[4] P. Chlubná, W. J. Roth, A. Zukal, M. Kubů, J. Pavlatová, *Catal Today*, **2012**, 179, 35.

[5] W. J. Roth, T. Sasaki, K. Wolski, Y. Song, D. M. Tang, Y. Ebina, R. Ma, J. Grzybek, K. Kalahurska, B. Gil, M. Mazur, S. Zapotoczny, J. Cejka, *Sci. Adv.*, **2020**, 6, eaay8163.

[6] V. Zholobenko, C. Freitas, M. Jendrlin, P. Bazin, A. Travert, F. Thibault-Starzyk, *J. Catal.*, **2020**, 385, 52.

[7] J. Grzybek, W. J. Roth, B. Gil, A. Korzeniowska, M. Mazur, J. Cejka, R. E. Morris, *J. Mater. Chem. A*, **2019**, 7, 7701.

[8] K. Góra-Marek, K. Tarach, M. Choi, *J. Phys. Chem. C*, **2014**, 118, 12266.

[9] M. Shamzhy, F. S. d. O. Ramos, *Catal Today*, **2015**, 243, 76.

[10] M. Thommes, *Chem. Ing. Tech.*, **2010**, 82, 1059.

[11] M. Thommes, K. Kaneko, A. V. Neimark, J. P. Olivier, F. Rodriguez-Reinoso, J. Rouquerol, K. S. W. Sing, *Pure Appl. Chem.*, **2015**, 87, 1051.

[12] O. L. J. Gijzeman, A. J. M. Mens, J. H. van Lenthe, W. J. Mortier, B. M. Weckhuysen, in *Studies in Surface Science and Catalysis*, Vol. 154 (Eds: E. van Steen, M. Claeys, L. H. Callanan), Elsevier, **2004**.

[13] S. R. Bare, A. Knop-Gericke, D. Teschner, M. Hävacker, R. Blume, T. Rocha, R. Schlögl, A. S. Y. Chan, N. Blackwell, M. E. Charochak, R. ter Veen, H. H. Brongersma, *Surf. Sci.*, **2016**, 648, 376.

[14] J. Stoch, J. Lercher, S. Ceckiewicz, *Zeolites*, **1992**, 12, 81.

[15] R. Verma, C. Singhvi, A. Venkatesh, V. Polshettiwar, *Nat. Commun.*, **2024**, 15, 6899.

[16] M. Todea, E. Vanea, S. Bran, P. Berce, S. Simon, *Appl. Surf. Sci.*, **2013**, 270, 777.

[17] B. Xue, T. Yi, D. Li, F. Li, F. Luo, *New J. Chem.*, **2022**, 46, 23268.